Existence domain of the compressive ion acoustic super solitary wave in a two electron temperature warm multi-ion plasma

S. V. Steffy[a] and S. S. Ghosh[b]
Indian Institute of Geomagnetism, Navi Mumbai, India

(Received 29 June 2017; accepted 25 August 2017; published online 20 September 2017)

The transition of an ion acoustic solitary wave into a "supersoliton," or a super solitary wave have been explored in a two electron temperature warm multi-ion plasma using the Sagdeev pseudopotential technique. It is generally believed that the ion acoustic solitary wave can be transformed to a super solitary wave only through a double layer. The present work shows that the transition route of an ion acoustic solitary wave to a super solitary wave is not unique. Depending on the electron temperature ratio, a regular solitary wave may transform to a super solitary wave either *via* the double layer, or through an extra-nonlinear solitary structure whose morphology differs from that of a regular one. These extra-nonlinear structures are associated with a fluctuation of the charge separation within the potential profile and are named as "variable solitary waves." Depending on these analyses, the upper and lower bounds of a super solitary wave have been deciphered and its existence domain has been delineated in the parametric space. It reveals that super solitary waves are a subset of a more generalized class of extra-nonlinear solitary structures called variable solitary waves. *Published by AIP Publishing.* [http://dx.doi.org/10.1063/1.4993511]

I. INTRODUCTION

The first time the concept of supersolitons came forth when, in 2012, Dubinov and Kolotkov[1] were working on a five component plasma comprising of electrons, positrons, positive and negative ions, and dust particles. In their analysis they obtained a new form of solitary waves which have larger amplitudes than usual. To distinguish them from other Regular Solitary Waves (RSWs), they coined the term "supersoliton." They were called "super" because of their extraordinary large amplitudes which are typically larger than the corresponding Double Layers (DLs). As they have larger amplitudes, the conventional methods like the Korteweg-de Vries (KdV) equation are not applicable for them; neither they have any analytical formalism like a traditionally known soliton. Instead, they are primarily identified by the additional subwell, or local extrema, in the conventional Sagdeev pseudopototential profile corresponding to an otherwise RSW solution. This has prompted us to propose a generalization of the nomenclature as Super Solitary Waves (SSWs) instead of "supersolitons."

Initially it was believed that the SSWs are an artefact of complicated plasma models which have at least five or four species of particles. It was further believed that the extra subwell in the pseudopotential arises due to tweaking of several plasma parameters which are available in such kinds of exotic multi-species plasmas. Soon after, Verheest *et al.*[2] confirmed that a minimum three component plasma is enough to support these extra-nonlinear solutions. Many more theoretical studies followed[3–13] which obtained SSWs for different plasma systems. These analytical results suggest that the proposition of SSWs is more realistic and fairly regular rather than to be an artefact. It is well known that a three component plasma is also necessary to support a rarefactive (negative amplitude) ion acoustic solitary wave or a DL while a two component plasma cannot sustain either of these structures. This condition holds true for an SSW as well. In that sense, SSWs are merely another candidate for a fully nonlinear localized structure, like rarefactive ion acoustic solitary waves or DLs.

Solitary waves and DLs have been studied extensively for last few decades, but there was never any report of structures like SSWs in the past.[14] The apparent fallacy may be explained by the very narrow and delicate balance of plasma parameters needed to sustain an SSW solution. It is this extremely narrow parameter regime for the existence domain of SSWs which makes their detection difficult. Albeit of such a selective condition, a recent simulation result showed that the SSWs are extremely stable structures.[15] It also reports an extra steepening prior to its formation which indicates that they are highly nonlinear solutions as predicted earlier.[1]

It is well known that the existence domain of a compressive (i.e., positive amplitude) ion acoustic solitary wave terminates due to steepening and wave breaking[16] while for a rarefactive ion acoustic wave, it terminates with a corresponding DL solution.[17] Ghosh and Iyengar[18] have shown that the inclusion of a very small concentration of sufficiently cooler electrons may generate compressive ion acoustic DLs. Depending on the termination process, they argued that the existence domain of the compressive ion acoustic solitary wave has two distinct regions or "phases" where the solutions are terminated either by a wave steepening (phase A, region A and B1 in Ref. 18), or DL (phase B, region B2 in Ref. 18). They have also shown that the transition from Phase "B" to Phase "A" leads to a sharp discontinuity and the onset of SSWs.

While existence domains for RSWs are well known and well studied across different plasma models, little is known

[a]Electronic mail: steffy13@iigs.iigm.res.in
[b]Electronic mail: sukti@iigs.iigm.res.in

so far for that of SSWs. Recent research studies highlighted the conditions and the processes for the occurrence of SSWs.[5,18–20] Verheest *et al.*[5] investigated the occurrence of ion acoustic "supersolitons" in a dusty plasma with stationary negative dusts, cold fluid protons, and Cairns distributed electrons. They critically analyzed the existence of SSWs beyond the DL. From their analysis they inferred that an SSW occurs after a DL and they argued that, after SSW, ordinary solitary waves are formed due to the coalescence of the extrema of the pseudopotential. Shortly after them, Maharaj *et al.*[19] also concluded that the lower limit of SSWs is a DL. The process of coalescence of the subwells has also been confirmed in our recent work[20] where we have further quantified it by assigning some typical characteristic values for the cold to hot electron temperature ratios. It revealed the deterministic role of the electron temperature ratio which decides the particular type of the limiting solution. In this process, we have also identified the different intermediate structures, like a Curve of Inflection (CoI) and Variable Solitary Waves (VSWs), other than SSWs. This calls for a reexamination of the present understanding that an SSW necessarily emerges out of a DL. It also becomes necessary to explore the association of SSWs with these intermediate extra-nonlinear structures. To quantify the possible correlations, here we have studied the transition of RSW to SSW with varying cooler electron concentrations. The corresponding values of the electron temperature ratio have been chosen according to the limiting solutions highlighted in our previous analysis.[20] As a result, we have been able to identify a set of characteristic values for the cooler electron concentration which affects the transition route to any particular limiting solution. It also confirms that there is no unique route for the onset of an SSW. The study helped us to delineate the overall existence domain of SSWs.

The present paper is organized as follows. The model and formulation are explained in Sec. II, Sec. II A representing the derivation of the Sagdeev pseudopotential while Sec. II B analyzes the properties and conditions for its derivatives. Section III delineates the overall existence domain of SSW by studying the conditions for its onset. Section III A studies the different routes to the limiting solution for the varying electron temperature ratio considering two different heavier ion concentrations (Secs. III A 1 and III A 3) and the results are further analyzed and compared with a regular variation for RSWs (Sec. III A 2). The study leads to Sec. III B which categorizes two distinct types of transition routes for the onset of an SSW while Sec. III C summarizes the existence domains for these extra-nonlinear structures in a parametric regime determined by the relative electron temperatures and concentrations. The overall conclusion has been given in Sec. IV.

II. FORMULATION

A. Derivation of the Sagdeev pseudopotential

The theoretical model has considered the plasma to be infinite, homogeneous, collisionless and unmagnetized, which consists of two warm ions (lighter and heavier) and two temperature electrons. Recalling the basic equations and the parameters explained in Varghese and Ghosh,[20] the lighter (n_{il}) and the heavier (n_{ih}) ion densities are given by

$$n_{il} = \frac{\alpha_l}{2\sqrt{3\sigma_l}}\left[\left((M+\sqrt{3\sigma_l})^2 - 2\Phi\right)^{\frac{1}{2}} - \left((M-\sqrt{3\sigma_l})^2 - 2\Phi\right)^{\frac{1}{2}}\right],$$

$$n_{ih} = \frac{\alpha_h}{2\sqrt{3\sigma_h}}\left[\left(\left(\frac{M}{\sqrt{Q}}+\sqrt{3\sigma_h}\right)^2 - 2\Phi\right)^{\frac{1}{2}} - \left(\left(\frac{M}{\sqrt{Q}}-\sqrt{3\sigma_h}\right)^2 - 2\Phi\right)^{\frac{1}{2}}\right],$$

respectively. We are assuming the electrons are following Boltzmann distribution and are separately in thermal equilibrium. The total electron density is given as

$$n_e = n_{ec} + n_{ew} = \mu e^{\frac{\Phi}{\mu+\nu\beta}} + \nu e^{\frac{\beta\Phi}{\mu+\nu\beta}},$$

where the subscripts i, e, l, h, c, and w represent ions, electrons, lighter and heavier ions, and cooler and warmer electrons, respectively. M is the wave Mach number, Q is the lighter to heavier ion mass ratio ($Q = \frac{m_{il}}{m_{ih}}$), where m_{il} and m_{ih} are the mass of lighter and heavier ions, respectively, and β refers to the cold to hot electron temperature ratio ($\beta = \frac{T_{ec}}{T_{ew}}$). The normalized ion temperatures are $\sigma_j\left(=\frac{T_j}{T_{eff}}\right)$, normalized by the effective electron temperature $T_{eff}\left(=\frac{T_{ec}T_{ew}}{\mu T_{ew}+\nu T_{ec}}\right)$, where T_j is the ion temperature, j = il and ih, and $T_{ew}(T_{ec})$ are the temperatures of warmer (cooler) electrons, respectively. All number densities are normalized by the total equilibrium ion density $n_0(=n_{il}+n_{ih})$, which gives the corresponding ambient densities, *viz.*, α_l, α_h, μ, and ν, for lighter ions, heavier ions, cooler electrons and warmer electrons, respectively. The velocities, time, and length are normalized by the lighter ion acoustic speed $c_{isl}\left(=\sqrt{\left(\frac{T_{eff}}{m_{il}}\right)}\right)$, inverse of ion plasma frequency $\omega_{pil}^{-1}\left(=\left(\frac{n_0e^2}{\epsilon_0 m_{il}}\right)^{-\frac{1}{2}}\right)$, and the effective Debye length $\lambda_{eff}\left(=\left(\frac{\epsilon_0 T_{eff}}{n_0e^2}\right)^{\frac{1}{2}}\right)$, respectively. The pressure p_{ij}, $(j = h \text{ and } l)$, is normalized by the ion equilibrium pressure p_0 $(=n_0T_i)$, where T_i $(=\alpha_l T_{il}+\alpha_h T_{ih})$ is the net effective temperature of ions, and potential ϕ is normalized by $\frac{T_{eff}}{e}$.

The corresponding Poisson's equation is given by,

$$\frac{\partial^2\Phi}{\partial x^2} = n_{ec} + n_{ew} - n_{ih} - n_{il}. \tag{1}$$

According to the Sagdeev pseudopotential technique

$$\frac{\partial^2\Phi}{\partial\eta^2} = n_i - n_e = -\frac{\partial\Psi(\Phi)}{\partial\Phi}, \tag{2a}$$

$$\text{which leads to,} \quad \frac{1}{2}\left(\frac{\partial\Phi}{\partial\eta}\right)^2 + \Psi(\Phi) = 0, \tag{2b}$$

where $\Psi(\Phi)$ is the Sagdeev pseudopotential.

Integrating the Poisson's equation with ion and electron densities, we have obtained the Sagdeev pseudopotential $\Psi(\Phi)$ for two electron temperature warm multi-ion plasma which is given as[20]

$$\begin{aligned}\Psi(\Phi) = -\Bigg[&(\mu+\nu\beta)\left(\mu\left(\exp\frac{\Phi}{\mu+\nu\beta}-1\right)\right.\\&\left.+\frac{\nu}{\beta}\left(\exp\frac{\beta\Phi}{\mu+\nu\beta}-1\right)\right)\\&+\frac{\alpha_l}{6\sqrt{3\sigma_l}}\left(\left[(M+\sqrt{3\sigma_l})^2-2\Phi\right]^{\frac{3}{2}}-(M+\sqrt{3\sigma_l})^3\right.\\&\left.-\left[(M-\sqrt{3\sigma_l})^2-2\Phi\right]^{\frac{3}{2}}+(M-\sqrt{3\sigma_l})^3\right)\\&+\frac{\alpha_h}{6\sqrt{3\sigma_h}}\left(\left[\left(\frac{M}{\sqrt{Q}}+\sqrt{3\sigma_h}\right)^2-2\Phi\right]^{\frac{3}{2}}\right.\\&-\left(\frac{M}{\sqrt{Q}}+\sqrt{3\sigma_h}\right)^3-\left[\left(\frac{M}{\sqrt{Q}}-\sqrt{3\sigma_h}\right)^2-2\Phi\right]^{\frac{3}{2}}\\&\left.+\left(\frac{M}{\sqrt{Q}}-\sqrt{3\sigma_h}\right)^3\right)\Bigg].\end{aligned} \tag{3}$$

In order to obtain the solitary wave solution, and to ensure the recurrence of the initial state, $\Psi(\Phi)$ of Eq. (3) must satisfy the following boundary conditions:

$$\begin{aligned}\Psi(\Phi=0)=\left.\frac{\partial\Psi}{\partial\Phi}\right|_0=0;\quad \frac{\partial^2\Psi(0)}{\partial\Phi^2}<0;\\ \Psi(\Phi_0)=0;\quad \frac{\partial\Psi(\Phi_0)}{\partial\Phi}\neq 0.\end{aligned} \tag{4}$$

This also implies that $\Psi(\Phi)<0$ for $0<\Phi<\Phi_0$ where Φ_0 is the amplitude of the solitary waves.

B. Derivatives of the Sagdeev pseudopotential and additional conditions

Apart from all these conditions in Eq. (4), an RSW appears to satisfy the additional condition[20]

$$\frac{\partial^3\Psi}{\partial\Phi^3}>0,\quad \text{for } 0\le\Phi\le\Phi_0. \tag{5}$$

For all Other Solitary Waves (OSWs), including VSWs, SSWs, and CoIs, the 3rd derivative of Eq. (3) (i.e., $\frac{\partial^3\Psi}{\partial\Phi^3}$) fluctuates between positive and negative values within the range indicating a variability in the charge separation (Δn) within the localized structure (Eq. 2a). We may recall that an SSW is defined by the additional extrema of $\Psi(\Phi)$ and bounded by CoI. A CoI is characterized by a "point of inflection" at $\Phi=\Phi_{CoI}$ where

$$\frac{\partial\Psi(\Phi_{CoI})}{\partial\Phi}=\frac{\partial^2\Psi(\Phi_{CoI})}{\partial\Phi^2}=0;\qquad 0<\Phi_{CoI}<\Phi_0. \tag{6}$$

Typically, the pseudopotential profile of an SSW exhibits 4 extrema while that for a CoI is 3. An RSW, and a generalized VSW (gVSW) other than SSW or CoI, both have two extrema only, but the latter (gVSW) differs from an RSW as it does not satisfy Eq. (5). By a gVSW we mean that subset of OSWs which excludes more specific class of solutions like SSW and CoI, but still observes an extra wiggle in the corresponding pseudopotential profile. In other words, for a gVSW, though the charge separation (Δn) fluctuates but it always remains positive and finite near the vicinity of the maximum amplitude (Eq. 2a).[20]

For a DL, there is no recurrence of the initial state. The last boundary condition of Eq. (4) thus modifies to the following:

$$\Psi(\Phi_d)=0;\qquad \frac{\partial\Psi(\Phi_d)}{\partial\Phi}=\Delta n_d=0, \tag{7}$$

where Φ_d is the amplitude of the DL and Δn_d is the charge separation at Φ_d.

For our model, the compressive positive amplitude solitary wave should further satisfy the energy condition given by

$$\Phi_0<\frac{1}{2}\left(M-\sqrt{(3\sigma_l)}\right)^2;\quad \Phi_t=\frac{1}{2}\left(M-\sqrt{(3\sigma_l)}\right)^2, \tag{8}$$

Φ_t being the terminating amplitude beyond which $\Psi(\Phi)$ becomes complex and the wave breaks.[16]

III. RESULTS AND DISCUSSION

A. Different transition routes for OSW

Lately, it has become evident that the electron temperature ratio (β) plays a crucial role in determining all kinds of OSW solutions.[18,20] In our previous work, we have defined two characteristic β values, namely, β_s and β_v, respectively, which determine the overall parameter domain for OSWs ($\beta_s\le\beta\le\beta_v$). The former one ($\beta_s$) indicates the onset of an SSW while the latter (β_v) denotes the upper boundary of β supporting any kind of OSW as the limiting solution. Apart from the onset of the SSW, β_s is also associated with the very sharp and discontinuous phase transition between phases A and B (Sec. I), where for the latter the solitary wave terminates to DL.[18] So far all our analyses were restricted to the limiting value of μ ($=\mu_l$) (Ref. 18) which showed that, for $\beta_s\le\beta\le\beta_v$, the terminating OSW solution shifts from SSW to CoI, and then to gVSW, for increasing β. This immediately poses the question whether the route to the terminating solution remains unique, or varies with the change in the parameter regime. It is generally believed that an RSW may transform to an SSW *via* DL. We were curious to know how a gVSW may fit in this scheme of the transitional process. While it is fairly straightforward to predict the emergence of a gVSW out of SSW from the coalescence of extrema of the latter one,[5,20] it is still unclear whether an SSW may transform to an RSW with a larger, or equal amplitude through such gVSWs.

To have a more systematic and generalized understanding of these features and to explore the above-mentioned questions more accurately, we have assumed a multi-ion plasma comprising of two singly charged ions with finite ion temperatures and two populations of electrons with different

temperatures. For the sake of our convenience, it is assumed that both the heavier and lighter ions are of same temperatures, i.e., $\sigma_l = \sigma_h = \sigma$, and it remains constant (i.e., $\sigma = 0.033$) throughout our analysis. It is also assumed that the plasma is mainly comprised of H^+ ions with a minority component of He^+ ions, keeping the mass ratio $Q = 1/4$ a constant. In the present work, we have focused our attention on the parameter regime which supports OSW solutions and is bounded between β_s and β_v (i.e., $\beta_s \leq \beta \leq \beta_v$). Choosing a set of representative values for β, we have tried to find out those characteristics μ values which determine the onset (offset) of the corresponding SSW or OSW. The results have further been compared with a similar analysis of RSW beyond the said regime (i.e., $\beta > \beta_v$). To establish a more generalized approach, we have considered two different concentrations of heavier ions, namely, $\alpha_h = 0.1$ (low) and $\alpha_h = 0.2$ (high), respectively and, for the sake of comparison, we have also kept the Mach number constant ($M = 1.06$), unless specified otherwise.

1. OSW ($\beta_s \leq \beta \leq \beta_v$; $\alpha_l = 0.9$)

Here we have chosen a low heavier ion concentration ($\alpha_h = 0.1$) and have selected five different β values to study the respective Sagdeev pseudopotential profiles with varying μ. Throughout our analysis, a dotted curve represents an RSW, a dashed curve represents a gVSW or a DL, a dash-dot curve denotes a CoI, and a solid curve corresponds to an SSW. For the sake of convenience, we have defined two parameter ranges for μ, namely, R_o ($\equiv \mu_i \leq \mu \leq \mu_f$) and R_s ($\equiv \mu_{s1} < \mu < \mu_{s2}$), which support OSWs and SSWs, respectively. Similarly, R_g ($\equiv \mu_{v1} < \mu < \mu_{v2}$) defines the range for gVSWs. The parameters μ_i (μ_f), μ_{v1} (μ_{v2}), and $\mu_{s1}(\mu_{s2})$ are the characteristic μ values denoting the onset (offset) of an OSW, a gVSW, and an SSW, respectively. Noting that a CoI may either be the n-type or the p-type, depending on the morphology of the pseudopotential, the corresponding μ values are defined as μ_n and μ_p, respectively. The difference between these two types is that the coalescence of extrema may occur either at the 1st subwell of the pseudopotential (n-type), or the 2nd (p-type).[20] Throughout our analysis, μ_l is that limiting μ value beyond which any solitary wave solution, including OSWs, terminates (i.e., $\mu_f = \mu_l$), and μ_d denotes the DL.

*a. **Case 1** ($\beta = \beta_s$):.* This β value corresponds to the aforementioned phase transition where the limiting solution transforms from a DL to an SSW. Figure 1 shows the Sagdeev pseudopotentials for different μ values, keeping all other parameters and β constant while Table I summarizes the solutions associated with different curves, marked by "j," j being 1, 2, 3, etc., along with their corresponding μ values (μ_j). The last column denotes the particular characteristic μ values for this regime. It clearly shows that an RSW (curve 1) transforms to an SSW (curve 3) *via* a DL (curve 2). The result is consistent with those obtained previously by Verheest *et al.*[21] and is supported by others.[6,9,19] The terminating solution is an SSW and the route to the terminating solution is as follows:

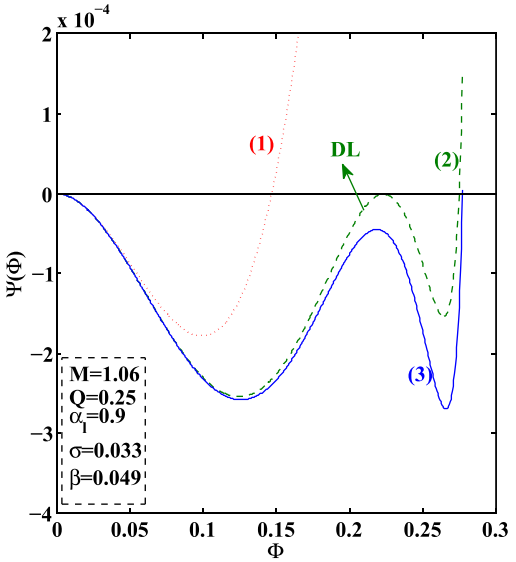

FIG. 1. Sagdeev pseudopotential profiles for Case 1, $\beta = 0.049$; Curves (1) RSW, (2) DL, and (3) SSW.

TABLE I. Summary of parameters: Case 1 ($\beta = 0.049$).

j	Type	μ_j	Characteristic μ
1	RSW	1×10^{-3}	$\mu_d = 1.285 \times 10^{-3}$
2	DL	1.285×10^{-3}	$\mu_l = 1.30042 \times 10^{-3}$
3	SSW	1.300×10^{-3}	

$$\text{RSW} \rightarrow \text{DL} \rightarrow \text{SSW};$$

$$R_o \equiv R_s \equiv \mu_d < \mu \leq \mu_l; \quad \mu_i = \mu_{s1} = \mu_d.$$

To complement our findings, we have plotted amplitude (Φ_0) *vs.* μ in Fig. 2 for different M and β. The intermediate DL solution between RSW and SSW readily explains the large jump in the amplitude (Φ_0) and the discontinuity. It also shows that the condition is not unique for any particular choice of the Mach number (M) but follows for other parameter regimes as well. It is well known that the amplitude of an RSW (dashed lines) increases with increasing M and μ[18]

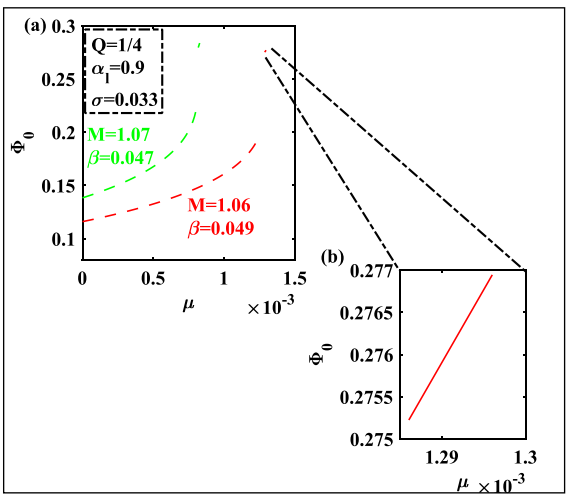

FIG. 2. Variation of amplitude (Φ_0) with μ for different M values; Case 1 transformation.

but decreases with β.[22] Eventually, with increasing M, the variation profile shifts to a lower μ and β value [Fig. 2(a)]. As M increases, not only the amplitude, but also the overall kinetic energy of the system increases,[17] leading to an increase in the terminating amplitude Φ_t (Eq. (8)), as well. It allows the condition for attaining an OSW to get adjusted to a lower β value [Fig. 2(a)]. The particular combination of $M-\beta$ ensures the optimum amplitude and allows the highly nonlinear solution to sustain. Interestingly, in Fig. 2(a), the variations of the amplitude after the discontinuity (solid lines) appears to be barely marginal for any of the parameters, *viz.*, M, μ, and β, compared to that prior to the discontinuity (dashed lines). We have already noticed that, for a particular regime supporting OSWs, the amplitude is often very close to its Φ_t and changes very slowly over the range of the parameters.[20] The same seems to hold true for a variation in M as well.

The delicate balance has made the range of μ values supporting OSWs much smaller than that for an RSW [Fig. 2(a)]. We have highlighted one of this variation for $M=1.06$ and $\beta=0.049$ in Fig. 2(b). It confirms a marginal increase in the amplitude with μ. According to Figs. 2(a) and 2(b), though the variation of Φ_0 *vs.* μ is monotonic before and after the discontinuity, the slope of the respective variation profiles differ significantly. Prior to the onset of the discontinuity, marked by μ_d, the slope shows a steep increase but it drops to a fairly moderate value after the discontinuity [Figs. 2(b)].

b. ***Case 2*** *($\beta \gg \beta_s$ but $\beta < \beta_{CoI}$):*. Here we have chosen a β value which is sufficiently away from the transition region ($\beta \gg \beta_s$) but closer to β_{CoI} and remains within $\beta_s \leq \beta \leq \beta_{CoI}$ where the terminating solution is an SSW. Figure 3 shows the respective Sagdeev pseudopotentials and Table II summarizes the solutions associated with different curves and their corresponding μ values as earlier (*viz.* Table I, Sec. III A 1 a), "j" being 1–4 in this case. All other parameters and legends remain the same as before. The particular route from RSW to SSW can now be summarized as,

TABLE II. Summary of parameters: Case 2 ($\beta=0.053$).

j	Type	μ_j	Characteristic μ
1	RSW	1×10^{-3}	$\mu_{v1}=1.5934\times10^{-3}$
2	gVSW	1.85×10^{-3}	
3	p-CoI	1.90547×10^{-3}	$(=\mu_p)$
4	SSW	1.97×10^{-3}	$\mu_l=1.9838\times10^{-3}$

$$\text{RSW} \rightarrow \text{gVSW} \rightarrow \text{p-CoI} \rightarrow \text{SSW};$$

$$R_o \equiv \mu_{v1} \leq \mu \leq \mu_l, \quad R_s \equiv \mu_p < \mu \leq \mu_l;$$

$$\mu_i = \mu_{v1}, \quad \mu_{s1} = \mu_p.$$

Clearly, in this case, the transformation of RSW to SSW is distinctly different from that of the previous one (Case 1, Sec. III A 1 a). Initially, as we increase μ, instead of a DL (curve 2, Fig. 1), there appears a "minor wiggle" in the pseudopotential (curve 2, Fig. 3) giving rise to a gVSW. The wiggle starts to arise in the otherwise smooth pseudopotential profile of RSW due to the fluctuation in the charge separation ($\Delta n = n_i - n_e$) and with a further increase in μ, it grows into a fully formed SSW (curve 4, Fig. 3) *via* p-CoI (curve 3, Fig. 3).[20] From an RSW to gVSW, the amplitude (Φ_0) also shows a large increase as well. This particular trend of transformation excludes the possibility of the existence of a DL between the RSW and gVSW, or gVSW and SSW. For the previous case (Sec. III A 1 a), from RSW the solution transforms to a DL where both the generalized electric field ($-\frac{\partial\Phi}{\partial\eta}$) and the charge separation ($\Delta n = \frac{\partial\Psi}{\partial\Phi}$) vanish at $\Phi = \Phi_d$ (Eq. (7)). As μ increases, the vanishing charge separation ($\Delta n = 0$) shifts to a nonzero electric field ($\frac{\partial\Phi}{\partial\eta} \neq 0$) giving rise to an SSW. For the present case, however, the generalized electric field always remain nonzero between $\Phi = 0$, and Φ_0 (the amplitude), excluding the end points. It is the onset of a minor fluctuation in the charge separation (cuve 2) which grows larger with increasing μ, giving rise to an extra "fold" or subwell in the pseudopotential and, eventually, leads to an SSW.

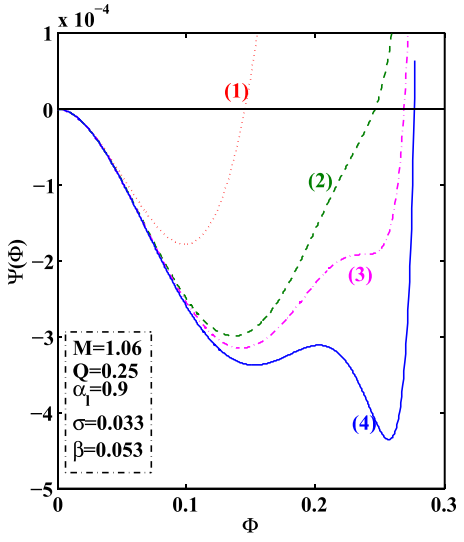

FIG. 3. Sagdeev pseudopotential profiles correspond to Case 2 transformation (1) RSW, (2) gVSW, (3) p-CoI, and (4) SSW.

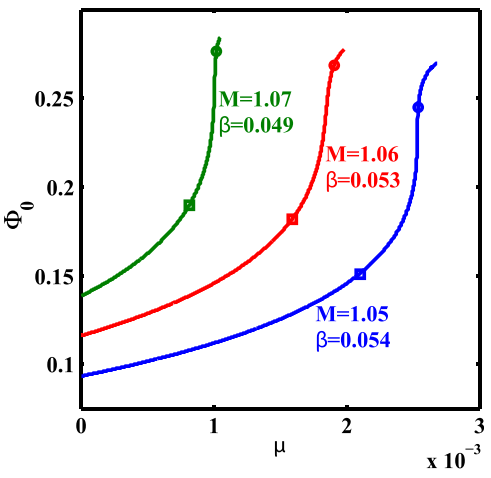

FIG. 4. The amplitude (Φ_0) variation with respect to μ for different Mach number (M) values for Case 2 transformation.

The difference between these two trends of transformation becomes further prominent in Fig. 4 where, following Case 1, we have plotted Φ_0 *vs.* μ for all the nonlinear structures assuming a certain sets of Mach number (M) and β. For each curve in Fig. 4, the "□" denotes the onset of the OSW ($\mu = \mu_i = \mu_{v1}$) while the "○" denotes the p-CoI ($\mu = \mu_p$). It readily shows a regular variation instead of a discontinuity as observed in the previous case. It confirms that there is a solitary wave solution, either an RSW or OSW, for each value of μ provided $0 < \mu \leq \mu_l$. The absence of the discontinuity also confirms that there is no DL solution within this range. A closer inspection reveals three distinct segments for each curve, denoted by (1), (2), and (3) in Fig. 4. For the first segment (segment (1), up to the "□"; $\mu < \mu_i$), and for a fixed value of β and M, Φ_0 increases gradually with μ but from $\mu = \mu_i$ onwards (segment (2), between the "□" and the "○"; $\mu_i \leq \mu \leq \mu_p$) it shows a steep accent and then again, beyond μ_p (segment (3), beyond the "○"; $\mu_p < \mu \leq \mu_l$), it decreases gradually. We may well conjecture that, as β is increasing from β_s to β_{CoI}, the gVSW solutions of segment (2) (i.e., $\mu_i \leq \mu \leq \mu_p$) start appearing there to bridge the gaps, or discontinuities, shown in Fig. 2(a) (Case 1, Sec. III A 1 a). The variation pattern observed in Fig. 4 was previously reported by Ghosh and Iyengar,[18] where they suggested that the steep accent of segment (2) occurs due to a kind of phase transition across $\beta = \beta_s$ between two distinctly different regions. In the present case, all the solutions belong to the same parametrical region and is away from the region of phase transition (i.e., $\beta \gg \beta_s$). In spite of a sharp change in the slope of the curve, there is no discontinuity either. The present analysis, thus, generalizes the previous findings.

In order to understand the variation of amplitude (Φ_0) with μ in Fig. 4 we have estimated the slopes of the different $M - \beta$ curves ($\frac{d\Phi_0}{d\mu}$), and plotted them for the corresponding ranges of μ (Fig. 5). It readily shows a steep increase, followed by even a sharper decrease in the slope for segment (2), while for segments (1) and (3) they vary gradually showing an opposite trend. For segment (1) (lower μ), the slope increases with μ while for segment (3) (i.e., $\mu \to \mu_l$), it decreases. In between these two segments, the very sharp peak indicates an unexpectedly large variation in Φ_0 over a

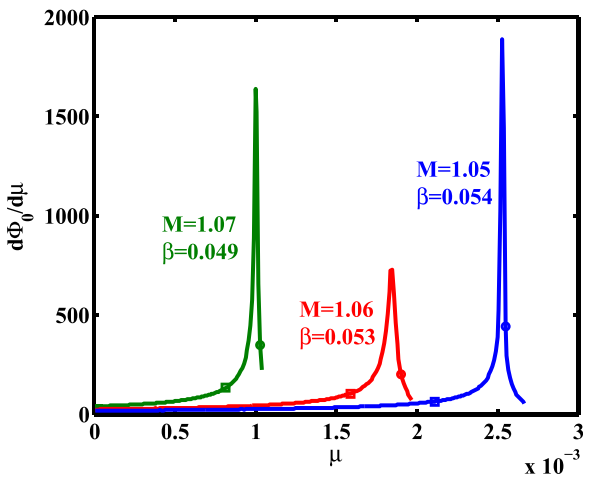

FIG. 5. Variation of $\frac{d\Phi_0}{d\mu}$ *vs.* μ for Case 2 transformation.

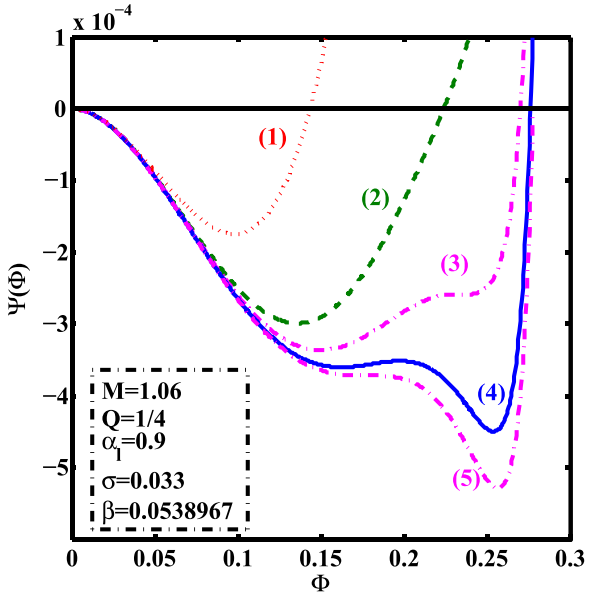

FIG. 6. Sagdeev pseudopotential profiles correspond to Case 3 transformation (1) RSW, (2) gVSW, (3) p-CoI, (4) SSW, and (5) n-CoI.

very small change in μ which hints to a "jump condition" similar to that reported earlier.[3,18] Though the extent of the sharpness of the peak varies quantitatively as M and β changes, the qualitative trend remains the same over our chosen set of parameters. Our latter analyses have confirmed this current trend throughout our chosen parameter regime. Between the regimes belonging to Case 1 and Case 2, respectively, we have identified a characteristic β value as $\beta = \beta_I$ beyond which there is no DL solution for the entire $\beta - \mu$ regime. Considering $M = 1.06$ and keeping all other parameters constant as chosen for Case 1, we have determined $\beta_I = 0.051$.

*c. **Case 3** ($\beta = \beta_{CoI}$).* As we increase β, the limiting solution transforms from SSW to a CoI. Figure 6 shows the Sagdeev psedopotentials for $\beta = \beta_{CoI}$ where $M = 1.06$ and other parameters remain the same. All the relevant μ values and the type of the solutions are listed in Table III. The overall transition is

$$\text{RSW} \to \text{gVSW} \to \text{p-CoI} \to \text{SSW} \to \text{n-CoI},$$

$$R_o \equiv \mu_{v1} \leq \mu \leq \mu_l; \quad R_s \equiv \mu_p < \mu < \mu_n;$$

$$\mu_i = \mu_{v1}, \quad \mu_{s1} = \mu_p, \quad \mu_{s2} = \mu_n = \mu_l.$$

This transition can be interpreted as the extension of the previous one (Case 2, Sec. III A 1 b) with an additional n-CoI solution for a larger amplitude. This also shows that both p-

TABLE III. Summary of parameters: Case 3 ($\beta = 0.0538967$).

j	Type	μ_j	Characteristic μ
1	RSW	1×10^{-3}	$\mu_{v1} = 1.77 \times 10^{-3}$
2	gVSW	2.05×10^{-3}	
3	p-CoI	2.08115×10^{-3}	$(= \mu_p)$
4	SSW	1.97×10^{-3}	
5	n-CoI	2.16154×10^{-3}	$(= \mu_n)$

CoI and n-CoI may be supported within the same parameter regime. Previously we showed that a CoI denotes the boundary of an SSW. Here we have found that, for this particular set of parameters, the p-CoI denotes the lower boundary of the SSW while the n-CoI denotes the upper. So, at $\beta = \beta_{CoI}$, the SSW is sandwiched between a p-CoI and an n-CoI. It also shows that the n-CoI has a larger amplitude, and hence a higher nonlinearity than p-CoI.

As mentioned in Case 2, the pseudopotentials in Fig. 6 themselves show that, as μ increases, the wiggles start to appear with a big "jump," or increase in the amplitude but after reaching a certain μ, the amplitude (Φ_0) becomes quite close to its terminating value ($\Phi \to \Phi_t$). With a further increase in μ the amplitude does not increase in the same rate as earlier but varies only marginally or becomes almost near-constant. A more detailed analysis of the variation of the amplitude will be discussed in the due course.

*d. **Case 4** ($\beta > \beta_{CoI}$ but $\beta \ll \beta_v$).* We have now chosen a β which is greater than β_{CoI} but remains close to it. In this regime ($\beta_{CoI} < \beta < \beta_v$), the solution terminates as a gVSW. In order to explain the types of transformation of nonlinear structures in that regime, we have plotted the Sagdeev pseudopotential profiles as shown in Fig. 7 while Table IV summarizes the relevant details. The transformations are similar to Case 3 (Sec. III A 1 c) and can be summarized as

$$\text{RSW} \to \text{gVSW}_m \to \text{p-CoI} \to \text{SSW} \to \text{n-CoI} \to \text{gVSW}_r;$$

$$R_o \equiv \ \mu_{v1} \le \mu \le \mu_l, \quad R_s \equiv \ \mu_p < \mu < \mu_n;$$
$$\mu_i = \mu_{v1}, \quad \mu_{s1} = \mu_p, \quad \mu_{s2} = \mu_n.$$

The major difference here from the previous one (Case 3, Sec. III A 1 c) is the appearance of two different bands of gVSWs, appearing before and after the regular SSW. We have marked them by two subscripts, *viz.* '*m*', for a smaller amplitude, and '*r*', for the larger one, respectively. It also shows that, with increase in β, the μ regime supporting a regular SSW shifts to a lower value. The SSW solutions are now clearly sandwiched between the p and n types of CoIs ($\mu_p < \mu < \mu_n$), forming a distinct subset within the overall range of VSW or OSW ($\mu_i < \mu < \mu_f$). This also shows that increase in β extends the overall range of OSW solutions.

TABLE IV. Value of parameters: Case 4 ($\beta = 0.055$).

j	Type	μ_j	Characteristic μ
1	RSW	1.5×10^{-3}	$\mu_{v1} = 2.01 \times 10^{-3}$
2	gVSW	2.2×10^{-3}	
3	p-CoI	2.30935×10^{-3}	$(= \mu_p)$
4	SSW	2.325×10^{-3}	
5	n-CoI	2.35517×10^{-3}	$(= \mu_n)$
6	gVSW	2.4×10^{-3}	$\mu_l = 2.4006 \times 10^{-3}$

*e. **Case 5** ($\beta \gg \beta_{CoI}$ but $\beta < \beta_v$).* Contrasting the previous case, we now have chosen a β which is far away from β_{CoI} but remains smaller than β_v. The terminating solution thus continues to be a gVSW. As usual, Fig. 8 shows the Sagdeev pseudopotentials and Table V gives the μ values. Here the most striking feature is that there is no SSW solution at all. It appears like both the p-CoI and n-CoI have merged together keeping only gVSWs as the available solution. The overall trend of transformations can now be summarized as a simple two step process, *viz.*

$$\text{RSW} \to \text{gVSW}; \quad R_o \equiv R_g \equiv \mu_{v1} \le \mu \le \mu_l; \quad \mu_i = \mu_{v1}.$$

This eventually reveals another characteristics β value, namely, $\beta = \beta_{II}$, beyond which there is no SSW solution for any value of μ. Therefore the range of the β value, which supports SSW, is bounded by $\beta_s \le \beta \le \beta_{II}$. Considering $M = 1.06$ and keeping all other parameters constant as chosen for above cases we have found $\beta_{II} = 0.056$.

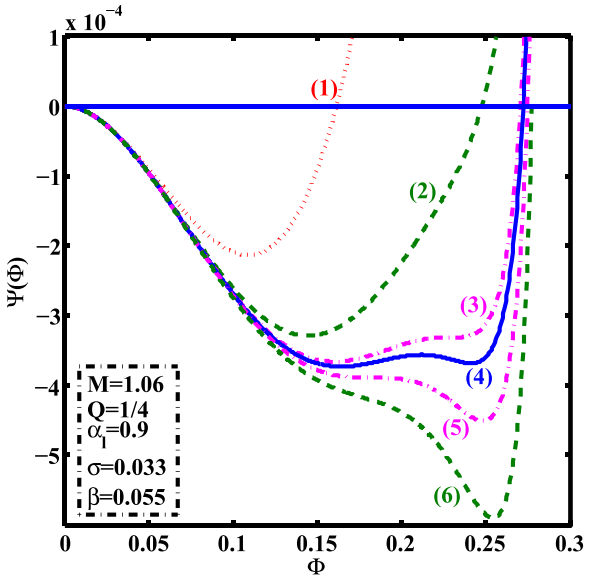

FIG. 7. Sagdeev pseudopotential profiles correspond to Case 4 transformation, (1) RSW, (2) gVSW, (3) p-CoI, (4) SSW, (5) n-CoI, and (6) gVSW.

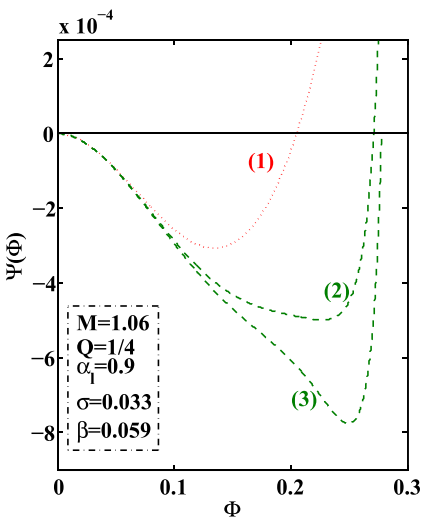

FIG. 8. Sagdeev pseudopotential profiles correspond to Case 5 transformation, (1) RSW, (2) gVSW, and (3) gVSW.

TABLE V. Summary of parameters: Case 5 ($\beta = 0.059$).

j	Type	μ_j	Characteristic μ
1	RSW	2.00×10^{-3}	
2	gVSW	3.3×10^{-3}	$\mu_{v1} = 3.06 \times 10^{-3}$
3	gVSW	3.42×10^{-3}	$\mu_l = 3.43 \times 10^{-3}$

2. RSW (Case 6: $\beta > \beta_v$; $\alpha_L = 0.9$)

It is known that, for $\beta > \beta_v$, the terminating solution is an RSW. Here we have chosen a β ($= 0.069$) which is only slightly greater than β_v ($= 0.067$). Figure 9 shows a set of Sagdeev pseudopotentials with varying μ, but fixed β. It reveals only RSW solutions, but no OSWs. This further confirms that, for $\beta > \beta_v$, not only the limiting one but also all other solitary wave solutions are RSWs and no OSW exists for any value of μ provided all other parameters, *viz.*, M, σ, Q, and α_l, remain constant (Sec. III A 1).

According to Case 4 (Sec. III A 1 d) we have observed that, with an increase (decrease) in μ, there is a gradual coalescence of extrema for the SSW giving rise to an n (p) type of CoI and then, with a further increase (decrease) in the parameter, it turns to a gVSW$_r$ (gVSW$_m$), respectively. As μ decreases further, the gVSW$_m$ merges to an RSW while an increase in μ leads the gVSW$_r$ to the wave breaking (Eq. (8)) and the solution ceases to exist. A similar trend continues for all the previous cases (Cases 1–5, Sec. III A 1) where, for the lower end ($\mu < \mu_{v1}$), the solution merges with an RSW but at the upper end it turns to be the limiting solution (i.e., $\mu = \mu_{v2} = \mu_l$). This poses the question whether it is possible for a gVSW to merge to an RSW with a larger amplitude. Our analysis shown in Fig. 9, however, rules out any such possibility. It also confirms that, though increase in μ indicates a gradual coalescence of extrema, the gVSW never actually transforms to an RSW with a larger amplitude. Whether this trend continues for any general class of model requires a more detail parametric analysis. For our choice of model, however, $\beta = \beta_v$ confirms the boundary of, not only the limiting, but all kinds of OSWs.

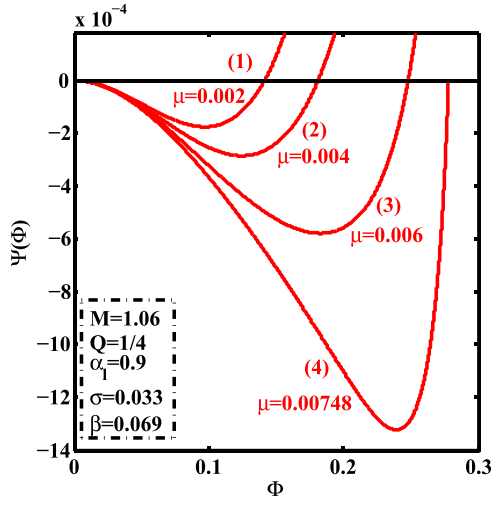

FIG. 9. Sagdeev pseudopotential profiles for RSWs (Case 6, $\beta = 0.069$).

Following Case 2 (Sec. III A 1 b), we have plotted Φ_o *vs.* μ and the variations of their slopes with μ in Figs. 10(a) and 10(b), respectively. We have chosen three selected values for $M - \beta$. It readily shows three segments of the amplitude variation (Sec. III A 1 b), namely, increase in the slope, a peak and a drop or decrease in the slope following the peak [Fig. 10(b)]. The profiles depicting the variation of the slopes are almost bell shaped with a visible asymmetry due to their steeper decent from the peak. As expected, the range of μ values supporting RSW is the largest for $M = 1.05$ which has the lowest amplitudes. The corresponding slope shows least asymmetry and is the widest of the three, confirming a slow variation of the amplitude. As M increases (and β decreases), along with the amplitudes [Fig. 10(a)] the heights of the peaks for the profiles in Fig. 10(b) also increase while their widths decrease making them sharper. The range of μ supporting the solution shrinks while the drop in the slope following the peak becomes even steeper with increasing M.

A comparison between Figs. 5 and 10(b) shows that, though both reveal a similar qualitative trend for the slopes, the former shows a very spiky, almost 'δ' like profile which is drastically different from that observed in Fig. 10(b). To understand this trend in more detail and to complement our findings on OSWs (Secs. III A 1), we have summarized the variations of the amplitudes with μ for Cases 2–5 in Figs. 11(a)–11(d), respectively while Figs. 12(a)–12(d) show their respective variations of the slopes. As before, the "□" and "○" in Figs. 11(a)–11(d) mark the onset of gVSW ($\mu = \mu_{v1}$),

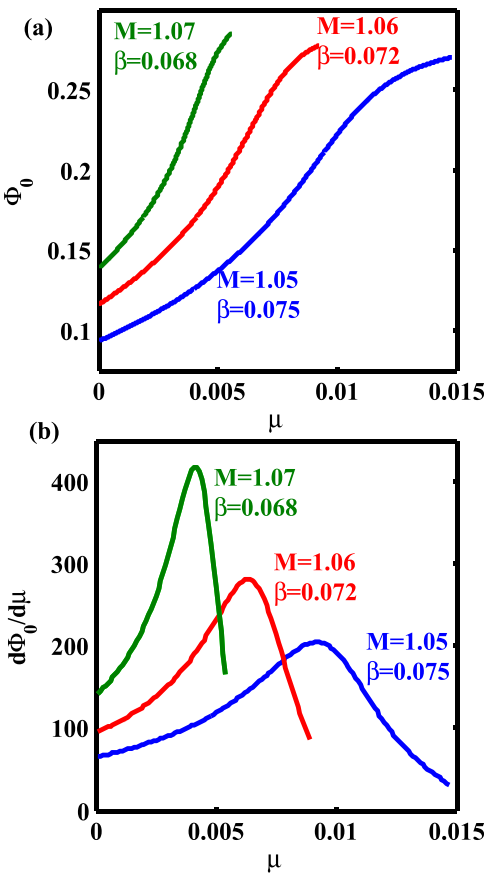

FIG. 10. (a) Variation of amplitude (Φ_0) with μ (b) Variation of $\frac{d\Phi_0}{d\mu}$ *vs.* μ, for RSW.

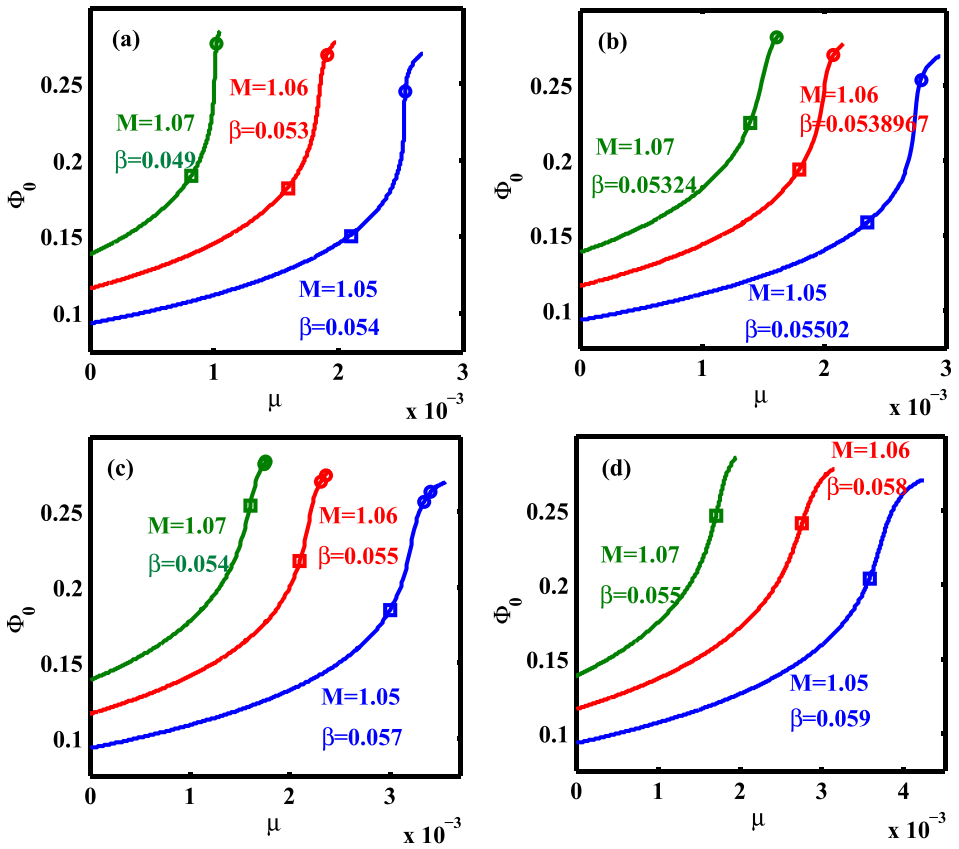

FIG. 11. Variation of Φ_0 with respect to μ for Cases 2–5.

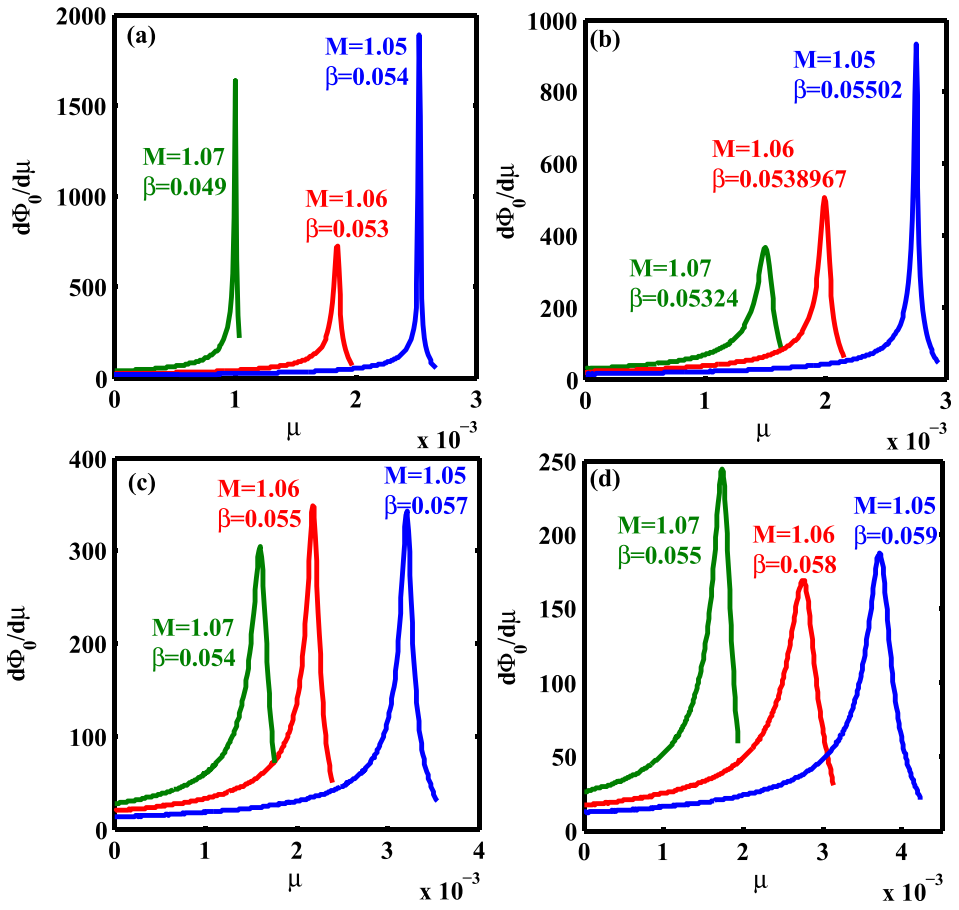

FIG. 12. $\frac{d\Phi_0}{d\mu}$ *vs.* μ corresponding to Fig. 11.

and p-CoI ($\mu = \mu_p$), respectively. For all the cases, the set of M values remain constant, *viz.*, $M = 1.05$, 1.06, and 1.07 while for Figs. (11) and (12), the corresponding β values have been chosen according to the prescribed limiting solutions (Sec. III A 1). It shows that the amplitude (Φ_0) increases with μ while both the amplitude (Φ_0) and the limiting amplitude (Φ_t) increases with M though the latter increases only marginally [Figs. 11(a)–11(d)]. The range of μ values decreases with increasing M and Φ_0. It also shows that, even with a small overall increase in β from Figs. 12(a) to 12(d), which is typically < 0.01, there is a drastic decrease ($\approx 90\%$) in the peak of the slopes. This is followed by a corresponding decrease in the sharpness, and smoothening of the profiles. Characteristically, an individual profile in Fig. 12(d) resembles that of Fig. 10(b) but, unlike the latter one, the former profiles do not show any regular trend for changing M and β. This trend follows for Figs. 12(a)–12(c) as well. More specifically, in Figs. 12(a) and 12(b), the largest peaks occur for $M = 1.05$ while in Fig. 12(d) they occur at $M = 1.07$. On the other hand, $M = 1.06$ corresponds to the lowest peak for Figs. 12(a) and 12(d) while for Figs. 12(b) and 12(c) $M = 1.07$ is the lowest. In Fig. 12(c), peaks corresponding to $M = 1.05$ and 1.06 are almost equal. The apparently arbitrary trend may be caused due to their delicate "jump conditions" (Sec. III A 1) which depends on the very minute combination of parameters. We further note that the "jump condition" takes place with the onset of gVSW, marked by "□"s in Figs. 11(a)–11(d) while beyond μ_p (marked by "○"), the amplitude turns near constant and the slope drastically drops to a very low value. The sharpest peak occurred at $M = 1.05$, $\beta = 0.054$ [Fig. 12(a)] where the profile looks like almost a δ function thanks to the near vertical increase in amplitude over a minute change in μ, as shown in Fig. 11(a).

3. Revisiting OSW ($\alpha_l = 0.8$)

We have previously observed that, as the heavier (lighter) ion concentration changes, morphology of the Sagdeev pseudopotential for the limiting solution at $\beta = \beta_{CoI}$ may also change from n-CoI ($\alpha_l = 0.9$) to p-CoI ($\alpha_l = 0.8$). This calls for a revisit of all our above mentioned analyses, *viz.*, Cases 1–6, (Secs. III A 1 a–e and III A 2) with an increased heavier ion concentration (lower α_l). For the sake of comparison, we keep all the other parameters same as that in the Sec. III A 1 while vary the lighter ion concentration from $\alpha_l = 0.9$ to 0.8, enhancing the contribution of the heavier ions. It has confirmed that the transitional processes as experienced previously for Cases 1 and 2 do not get affected by the change in the relative ion concentration. In other words, we may conclude that the transitional processes for the $\beta_s \le \beta < \beta_{CoI}$ regime remained the same throughout the selected range of α_l. The same holds true for Case 6, i.e., $\beta > \beta_v$ which revealed only the RSW solution as expected from our previous analysis. However, since the limiting solution itself differs at $\beta = \beta_{CoI}$, it is necessary to revisit it (*viz.*, Case 3, Sec. III A 1 c) for the reduced α_l. The details are as follows:

a. ***Case 7*** *($\beta = \beta_{CoI}$, $\alpha_l = 0.8$).* Figure 13 shows the Sagdeev pseudopotentials corresponding to $\beta = \beta_{CoI}$ while Table VI summarizes all their properties and corresponding

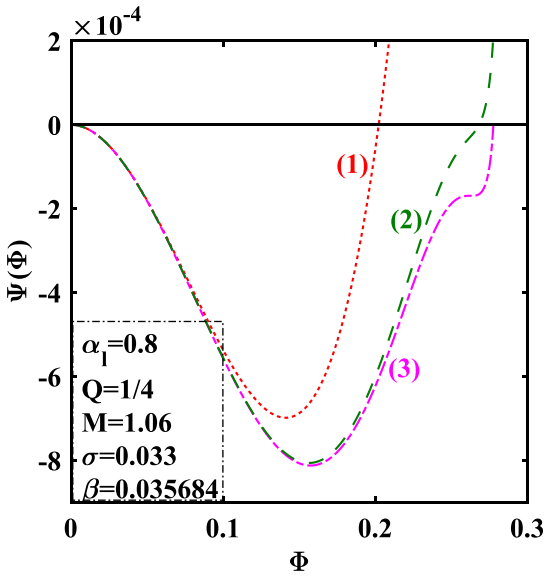

FIG. 13. Sagdeev pseudopotential profiles for Case 7 ($\alpha_L = 0.8$, $\beta = 0.035684$); Curves (1) RSW, (2) gVSW, and (3) p-CoI.

characteristic μ values. We recall that, for $\alpha_l = 0.9$ and $\beta = \beta_{CoI}$, the terminating solution was n-CoI and the RSW transformed into n-CoI through gVSW, p-CoI and SSW (Sec. III A 1). For $\alpha_l = 0.8$, however, the RSW transforms into p-CoI through gVSW but, unlike the previous one, it does not support any SSW. The overall transitional process now can be represented as

$$\text{RSW} \rightarrow \text{gVSW} \rightarrow \text{p-CoI};$$
$$R_o \equiv R_g \equiv \mu_{v1} \le \mu \le \mu_l; \quad \mu_i = \mu_{v1}; \quad \mu_p = \mu_l,$$

which excludes any SSW solution. This suggests that, as α_l decreases, the β regime supporting SSW shrinks to $\beta_s \le \beta < \beta_{CoI}$. This also indicates that the decrease in the value of α_l pushes the corresponding p-CoI solution to a larger μ, ultimately turning it into a limiting solution at β_{CoI}. It is this upward shifting of the p-CoI solution, rather than any direct influence of α_l on the morphology of the Sagdeev pseudopotential, which turned the limiting solution from an n-CoI to a p-CoI.

b. ***Case 8*** *($\beta_{\text{CoI}} < \beta < \beta_v$).* Contrary to $\alpha_l = 0.9$, where we could identify two distinct transitional patterns for the selected β range, (*viz.*, Cases 4 and 5), for $\alpha_l = 0.8$ there exists only one type of transition. The pattern resembles to that of Case 5 for $\alpha_l = 0.9$, making these two cases, *viz.*, Cases 5 and 8 equivalent to each other, i.e.,

$$\text{RSW} \rightarrow \text{gVSW};$$
$$R_o \equiv R_g \equiv \mu_{v1} \le \mu \le \mu_l; \quad \mu_i = \mu_{v1}.$$

TABLE VI. Summary of parameters: Case 7 ($\beta = 0.035684$).

j	type	μ_j	Characteristic μ
1	*RSW*	5×10^{-5}	
2	*gVSW*	1.13×10^{-4}	
3	*p-CoI*	1.157×10^{-4}	$\mu_p = \mu_l$

This further confirms that the β regime for SSW shrinks with reduced α_I. The parameter β_{II} shifts to the left and merges with β_{CoI} making the latter the uppermost boundary of β supporting SSW solutions. This naturally eliminates any n-CoI solution and gVSWs with larger amplitudes for $\alpha_I = 0.8$. There is also no equivalence for Case 4. Cases 7 and 8 together confirm that a p-CoI necessarily represent a lower boundary of SSW and always have a lower amplitude than the corresponding n-CoI. For both the parameter regime, p-CoI moves up to larger μ with the increasing β. For $\alpha_I = 0.9$, a p-CoI moves to a larger μ (e.g., Case 4) and then ultimately merges with n-CoI (e.g., Case 5) leaving only gVSWs as OSW solutions. In the present situation ($\alpha_I = 0.8$), in the absence of any n-CoI, a p-CoI moves up, up to the limiting solution (Case 7) and any SSW ceases to exist from and beyond that value of β ($\beta \geq \beta_{CoI}$).

B. Comparison of different transition routes for OSW

In Secs. III A 1 and III A 3, we have studied the transition of an RSW to SSW for the selected β ranges (*viz.*, Cases 1–5) and different α_I values (*viz.*, Cases 7 and 8). A closer inspection readily reveals that there are grossly two distinct types of transition routes, namely

Type I transition: RSW → DL → SSW; ($\beta_s \leq \beta \leq \beta_I$)
Type II transition: RSW → gVSW$_m$ → p-CoI →SSW → n-CoI → gVSW$_r$; ($\beta_I < \beta \leq \beta_{II}$)

Type I is identical to Case 1 (Sec. III A 1 a) whereas Type II resembles Case 4 (Sec. III A 1 d). All other cases arise from the truncation of Case 4 at different levels. Cases 2 and 3 got truncated after step 4 (SSW) and step 5 (n-CoI), respectively, while Cases 7 and 8 get truncated after step 3 (p-CoI) and step 2 (gVSW), respectively. All these truncations occur due to the energy condition (Eq. (8)). For Case 5, the intermediate segment from step 3 to 5 (i.e., p-CoI → SSW → n-CoI) vanishes due to the coalescence between p-CoI and n-CoI reducing the Type II transition to a two step process only. Hence all the other cases except Case 1 (i.e., Cases 2 – 8) may be considered as the subcategory of Type II transition.

The main difference between the Type I and Type II transitions is that the former one is associated with a DL where the latter involves a gVSW rather than a DL. Here, a DL or DL-like solution necessarily means that the charge separation (Δn) should vanish at its maximum amplitude (Eq. (7)) whereas all OSWs, including gVSWs, have a finite non-zero charge separation at Φ_0 (i.e., $\frac{\partial \Psi}{\partial \Phi} \neq 0$). So far, to our knowledge, there is no directly reported evidence of an SSW which is not associated with a DL, or DL-like solutions. Results from Verheest *et al.*,[5] however, have indicated a non-DL intermediate solution between RSW and SSW which they termed as a "triple root" solution. They argued that the particular solution emerges due to the coalescence of the adjacent two roots of the DL (*viz.*, Fig. 1, Sec. III A 1). Figure 14 shows a Sagdeev pseudopotential profile for our model which apparently resembles their triple root solution, i.e., the pseudopotential curve of the intermediate solution (curve 2, solid line) meets the zero axis with almost a "grazing incidence". The profile lies in between an RSW (curve 1, dotted line) and SSW (curve 3, dashed line). Figure 15 represents the corresponding profiles for the derivative. All the curves confirm a positive non zero charge separation (Δn) near the maximum amplitude (Φ_0). Interestingly, curve 2 does show a large drop in the charge separation (Δn) near Φ_0 but, after attaining a minimum value, which remains positive and non-zero, it once again shows an upward trend indicating another increase in charge separation (Δn) at the maximum amplitude (Φ_0). This excludes it from the category of any DL-like solution. Instead of turning to a DL, it will show a minor wiggle near the tip of the potential profile corresponding to curve 2 which, with increasing amplitude, will increase and shift towards a lower potential, eventually giving rise to a fully grown SSW (curve 3). In other words, as

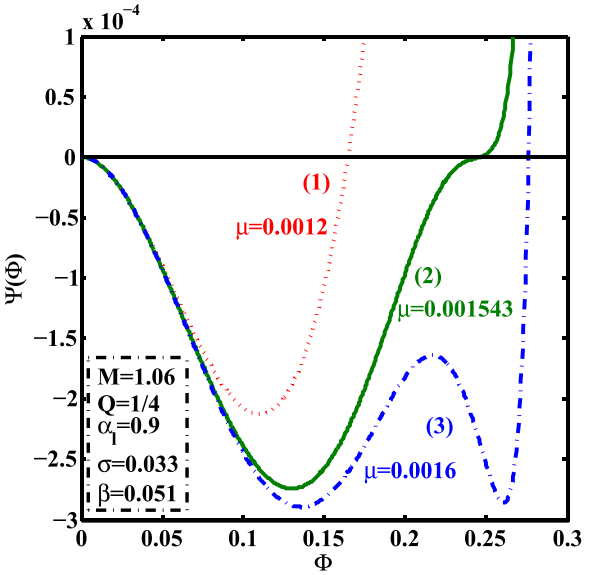

FIG. 14. Sagdeev pseudopotentials for (1) RSW, (2) "grazing incidence," and (3) SSW.

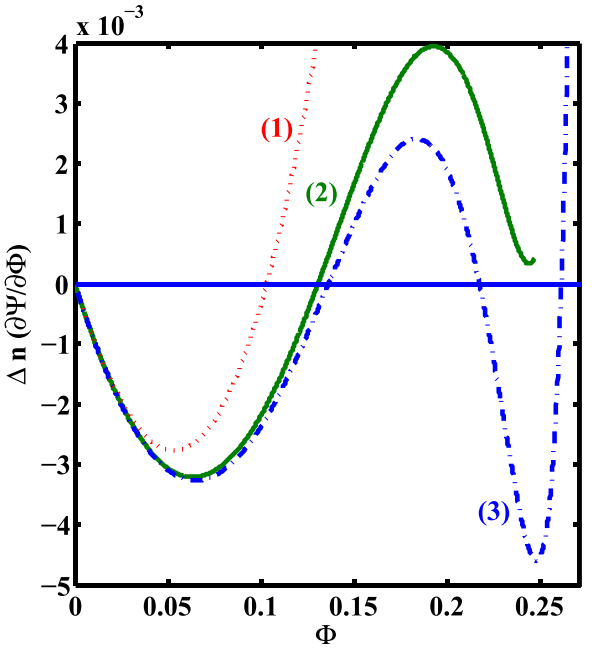

FIG. 15. Variation of $\frac{\partial \Psi}{\partial \Phi}$ with Φ corresponding to Fig. 14.

the amplitude (nonlinearity) increases, the wiggle shifts to a lower potential. According to our previous analysis,[20] and the characteristics of its derivative profile, the particular solution in Fig. 15 (curve 2) is thus categorized as a gVSW.

The trend of the Sagdeev pseudopotential curves in Fig. 14 already rules out any possibility of a DL solution between Curves 1 (RSW) and 2. The aforementioned upward trend in the charge separation (Δn) further eliminates the possibility of any DL after curve 2. This further confirms that the transition shown in Fig. 14 is that of Type II. From the large drop in the charge separation (Δn, Fig. 15) we may well conjecture that the RSW was tending to a DL but, somehow, it was prohibited and encountered a second steepening instead, which soon get balanced leading to an SSW solution. This appears to be consistence with the simulation result of Kakad *et al.*,[15] where they have noticed an extra large steepening prior to their SSW solution.

Though a Type II transformation has never been reported before, we have found it fairly regular and consistent for our model. To assess how exceptional it is vis-à-vis the Type I, we have delineated all the characteristic β values in Fig. 16 along with all the subregions (*viz.*, subregions "a" and "b") within the existence domain of OSWs ($\beta_s \leq \beta \leq \beta_v$). We have chosen $\alpha_l = 0.9$ and $M = 1.06$ and keep all other parameters constant. The subregion "a" denotes the range of β supporting SSW solutions while the subregion "b" comprises of the gVSW solution only. Focussing on SSW solutions (subregion "a"), we have found that, eventually, the region bounded between β_s and β_I ($\Delta\beta_I = \beta_I - \beta_s = 0.002$) is governed by the Type I transformation while that bounded between β_I and β_{II} ($\Delta\beta_{II} = \beta_{II} - \beta_I = 0.005$) is governed by the Type II transformation. It indicates that, of the overall β range observing SSW solutions (subregion a) only around 28% is governed by Type I while the rest major part follows a Type II transformation. In other words, a Type II transformation appears to be more common than that of Type I.

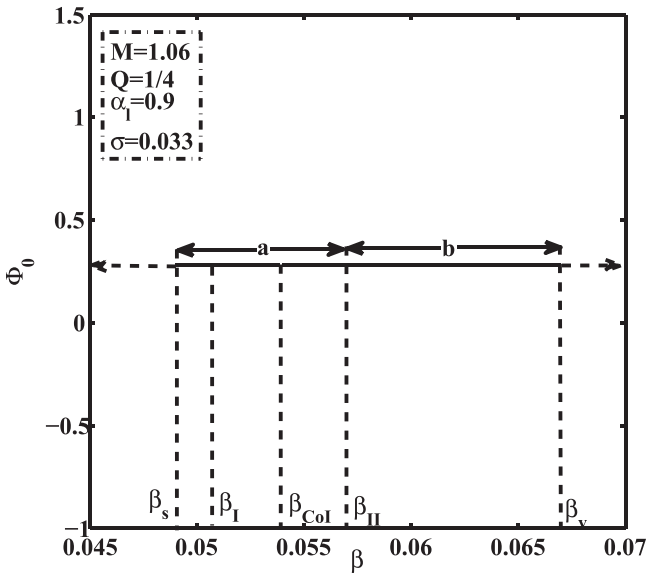

FIG. 16. The complete β regime supporting OSW solution.

C. Existence domain of extra-nonlinear structures

To find the existence domain of SSW, or OSW, it is necessary to determine the characteristic μ values associated with the onset (eg., μ_{s1}, μ_i) and offset (eg., μ_{s2}, μ_i) of the corresponding solution. We have observed that all these characteristic μ values vary significantly with varying β which in turn affects the particular ranges of R_s (R_o) supporting SSWs (OSWs), respectively. In Fig. 17(a) we have plotted the variations of the characteristic μ values with β for the complete range of β ($\beta_s \leq \beta \leq \beta_v$) where μ_l ($= \mu_f$) determines the upper boundary of the OSW solution. The green, solid lines represent the variations of μ_{s1} and μ_{s2}, the brown, dash-dot lines are for μ_i and μ_f ($=\mu_l$) while the blue, dashed line shows the variation of μ_d. To highlight different subregions, the vertical dotted lines mark the various characteristic values for β. The spindle shaped area bounded between the two solid lines, *viz.*, μ_{s1} and μ_{s2}, represents the existence domain of the SSW (R_s) in an overall $\mu - \beta$ regime. For the clarity, the region is further highlighted in Fig. 17(b). For a Type I transition, μ_{s1} is associated with a DL (i.e., μ_d) while for Type II, it is associated with a p-CoI (μ_p). The spindle converges to a point at both of its ends and the endpoints are determined by the lower (β_s) and upper (β_v) bounds of β. The range of the μ values appeared to be the largest around $\beta \approx \beta_{CoI}$ [Fig. 17(b)], but tapers down for both the directions. The dashed line shows the variation of μ_d representing the DL solution. For $\beta < \beta_s$ it determines the upper boundary of the RSW while beyond β_s and up to β_I ($\beta_s \leq \beta < \beta_I$) it merges with the lower boundary of R_s. As β increases further, i.e., $\beta_I \leq \beta \leq \beta_{II}$, the lower boundary of R_s is determined by the variation of μ_p for a p-CoI solution. The upper boundary, on the other hand, is determined by μ_l ($= \mu_f$, dash-dot curve) up to β_{CoI}, but from that point onward ($\beta_{CoI} < \beta \leq \beta_{II}$), it bifurcates towards a lower μ value ($\mu_{s2} < \mu_l$) and merges with the variation of μ_n for n-CoI. The lower bound, i.e., both μ_d and μ_p, increases monotonically with β though the former shows a comparatively slower rate of variation [Figs. 17(a) and 17(b)]. The rate of increase in the upper bound, on the other hand, slows down after β_{CoI} which eventually narrows down the existence domain.

While boundaries of SSW solutions are well marked, that for a gVSW is relatively blurred due to the seamlessly continuous and incremental transformations of an RSW to a gVSW. To minimise the confusion, we have explored the overall existence domain of OSW which comprises of all the types of the extra-nonlinear structures, including the SSW and the gVSW. The upper boundary of an OSW is uniquely defined by μ_l (Eq. (8)). We have estimated the lower bound of the OSW by delineating two characteristic μ values, *viz.*, μ_d (for Type I) and μ_{v1} (for Type II), respectively. The former one (μ_d) assumes that any such extra-nonlinear solution has a larger amplitude than the corresponding DL. The latter one (μ_{v1}) is associated with the onset of a gVSW and is that the lowest μ which does not satisfy Eq. (5). We have already shown that, for a Type II transition, and in the absence of a DL, the onset of an OSW is actually determined by that of a gVSW. On the basis of those aforementioned assumptions,

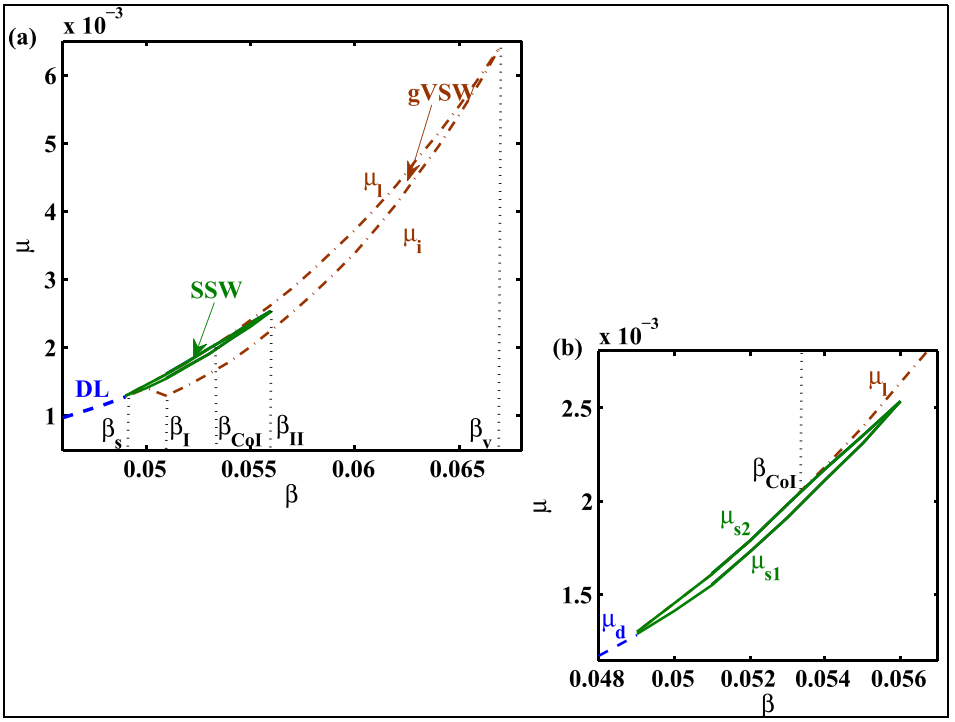

FIG. 17. (a) The overall existence domain of OSW (brown dash-dott lines) and SSW (green solid lines); the blue dashed line represents DL. (b) The highlighted existence domain of SSW (green solid lines); the brown dash-dotted line represents the upper limit of OSW and the blue dashed line represents DL.

conditions for the lower boundary of an OSW may thus formally be written as

$$\mu_i = \begin{cases} \mu_d & : \beta_s \le \beta < \beta_I \\ \mu_{v1} & : \beta_I \le \beta \le \beta_v. \end{cases} \quad (9)$$

The region bounded in between two dash-dot curves represents the complete existence domain for OSWs. It readily shows that the previously discussed SSW existence domain [R_s, solid curves; Figs. 17(a) and 17(b)] is considerably narrower than the overall R_o. It also confirms that SSWs are a subset of more general extra-nonlinear large amplitude solutions. Figure 17(a), along with Fig. 16, confirms the following condition in general,

$$R_s \ll R_g; \quad R_s \subset R_g; \quad \text{and} \quad R_g = R_o - R_s$$

We note that the lower boundary shows a significant initial dip in μ near $\beta \le \beta_I$ but beyond $\beta = \beta_I$, both the upper and lower bounds of R_o increases monotonically with increasing β. It appears that the lower bound increases more rapidly compared to the upper bound. The former gradually merges with the latter and an OSW solution ceases to exist beyond β_v. Unlike the upper boundary, which is quantitatively unique and determined without any ambiguity, the lower boundary of the OSW, or gVSW is comparatively more qualitative in nature. It, however, represents a fairly reliable trend of the variation. A more specific and quantitative study of the lower boundary is beyond the scope of the present work and will be communicated elsewhere.

IV. CONCLUSION

So far it was believed that an SSW is necessarily associated with a DL. Our analyses have confirmed that they may emerge out of a gVSW as well. A gVSW is an otherwise ordinary solitary wave which has a substantial fluctuation in the charge separation but observes an overall increase in it near the maximum amplitude. We have categorized the former transition as Type I and the latter as Type II. In this process we have identified two more characteristics β values, *viz.*, β_I (β_{II}) which determines the respective parameter regime observing Type I (Type II) transitions. We have further observed that, for a Type II transition, the SSW solution is bounded between a p-CoI (lower bound) and n-CoI (upper bound). Eventually, we have delineated the spindle shaped existence domain for the SSW in the $\mu - \beta$ regime. The very narrow area of the existence domain indicates that a very delicate balance is required to sustain an SSW solution. Though the relative densities and temperatures of the electrons primarily determines the existence domain of the SSW, an increase in the heavier ion concentration (α_h) inhibits the formation of SSWs and shrinks its existence domain.

The onset of an OSW is always associated with an abrupt increase in the amplitude (jump condition). In order to quantify it, we have implemented the derivative analysis for the variation of the amplitude with μ. The slope of the profile (i.e., $\frac{d\Phi_0}{d\mu}$) has shown a very characteristic feature along with a peak associated with the "jump condition". The peak is smooth and regular for an RSW, but turns spiky and irregular with an OSW. It arises due to the non-monotonic variation of the amplitude with μ.[18] The peaks provide a more quantitative estimate of the abruptness with which the amplitude increases.

To complete our analysis, we have also delineated the overall regime of the OSW. We have found that, for the Type II transition, the lower bound of the OSW is more qualitative due to its seamless and continuous merging with RSW. We have noticed that particular morphologies of a p and n type CoI ensure a higher nonlinearity when the "point of inflection" is associated with the first subwell of the

pseudopotential, i.e.,, Φ_0 (n-CoI) > Φ_0 (p-CoI). We have also confirmed that the amplitude of an RSW is always smaller than the corresponding gVSW. Our analysis is expected to enhance our understanding for these extra-nonlinear structures and their association with the otherwise regular solutions.

ACKNOWLEDGMENTS

The authors would like to acknowledge the Director of Indian Institution of Geomagnetism for the facilities and the encouragement for the completion of the work. The first author would like to thank her colleagues A. Lotekar and T. Kamalam for their valuable suggestions.

[1]A. E. Dubinov and D. Y. Kolotkov, IEEE Trans. Plasma Sci. **40**, 1429–1433 (2012).
[2]F. Verheest, G. S. Lakhina, and M. A. Hellberg, Phys. Plasmas **21**, 062303 (2014).
[3]A. E. Dubinov and D. Y. Kolotkov, Plasma Phys. Rep. **38**, 909–912 (2012).
[4]F. Verheest, M. A. Hellberg, and I. Kourakis, Phys. Plasmas. **20**, 012302 (2013).
[5]F. Verheest, M. A. Hellberg, and I. Kourakis, Phys. Rev. E **87**, 043107 (2013).
[6]M. A. Hellberg, T. K. Baluku, F. Verheest, and I. Kourakis, J. Plasma Phys. **79**, 1039–1043 (2013).
[7]O. R. Rufai, R. Bharuthram, S. V. Singh, and G. S. Lakhina, Phys. Plasmas. **21**, 082304 (2014).
[8]O. R. Rufai, R. Bharuthram, S. V. Singh, and G. S. Lakhina, Phys. Plasmas. **22**, 102305 (2015).
[9]S. V. Singh and G. S. Lakhina, Commun. Nonlinear Sci. Numer. Simul. **23**, 274–281 (2015).
[10]F. Verheest and M. A. Hellberg, Phys. Plasmas. **22**, 012301 (2015).
[11]C. P. Olivier, S. K. Maharaj, and R. Bharuthram, Phys. Plasmas. **22**, 082312 (2015).
[12]A. Paul and A. Bandyopadhyay, Astrophys. Space Sci. **361**, 172 (2016).
[13]D.-N. Gao, J. Zhang, Y. Yang, and W.-S. Duan, Plasma Phys. Rep. **43**, 1–5 (2017).
[14]T. K. Baluku, M. A. Hellberg, and F. Verheest, EPL **91**, 15001 (2010).
[15]A. Kakad, A. Lotekar, and B. Kakad, Phys. Plasmas **23**, 110702 (2016).
[16]R. B. White, B. D. Fried, and F. V. Coroniti, Phys. Fluids **15**, 1484 (1972).
[17]S. S. Ghosh and A. N. S. Iyengar, Phys. Plasmas **4**, 3204–3210 (1997).
[18]S. S. Ghosh and A. N. S. Iyengar, Phys. Plasmas. **21**, 082104 (2014).
[19]S. K. Maharaj, R. Bharuthram, S. V. Singh, and G. S. Lakhina, Phys. Plasmas **20**, 083705 (2013).
[20]S. S. Varghese and S. S. Ghosh, Phys. Plasmas **23**, 082304 (2016).
[21]F. Verheest, M. A. Hellberg, and I. Kourakis, Phys. Plasmas **20**, 082309 (2013).
[22]S. S. Ghosh and A. N. S. Iyengar, Phys. Scr. **61**, 361 (2000).